

Contents lists available at ScienceDirect

Petroleum Science

journal homepage: www.keaipublishing.com/en/journals/petroleum-science



Original Paper

Pressure transient characteristics of non-uniform conductivity fractured wells in viscoelasticity polymer flooding based on oil—water two-phase flow



Yang Wang *, Jia Zhang , Shi-Long Yang , Ze-Xuan Xu , Shi-Qing Cheng

National Key Laboratory of Petroleum Resources and Engineering, China University of Petroleum (Beijing), Beijing, 102249, China

ARTICLE INFO

Article history:
Received 26 August 2023
Received in revised form
16 October 2023
Accepted 18 October 2023
Available online 23 October 2023

Edited by Yan-Hua Sun

Keywords:
Polymer flooding
Non-Newtonian fluid
Non-uniform fracture conductivity
Two-phase flow
Pressure transient analysis

ABSTRACT

Polymer flooding in fractured wells has been extensively applied in oilfields to enhance oil recovery. In contrast to water, polymer solution exhibits non-Newtonian and nonlinear behavior such as effects of shear thinning and shear thickening, polymer convection, diffusion, adsorption retention, inaccessible pore volume and reduced effective permeability. Meanwhile, the flux density and fracture conductivity along the hydraulic fracture are generally non-uniform due to the effects of pressure distribution, formation damage, and proppant breakage. In this paper, we present an oil-water two-phase flow model that captures these complex non-Newtonian and nonlinear behavior, and non-uniform fracture characteristics in fractured polymer flooding. The hydraulic fracture is firstly divided into two parts: highconductivity fracture near the wellbore and low-conductivity fracture in the far-wellbore section. A hybrid grid system, including perpendicular bisection (PEBI) and Cartesian grid, is applied to discrete the partial differential flow equations, and the local grid refinement method is applied in the near-wellbore region to accurately calculate the pressure distribution and shear rate of polymer solution. The combination of polymer behavior characterizations and numerical flow simulations are applied, resulting in the calculation for the distribution of water saturation, polymer concentration and reservoir pressure. Compared with the polymer flooding well with uniform fracture conductivity, this non-uniform fracture conductivity model exhibits the larger pressure difference, and the shorter bilinear flow period due to the decrease of fracture flow ability in the far-wellbore section. The field case of the fall-off test demonstrates that the proposed method characterizes fracture characteristics more accurately, and yields fracture half-lengths that better match engineering reality, enabling a quantitative segmented characterization of the near-wellbore section with high fracture conductivity and the far-wellbore section with low fracture conductivity. The novelty of this paper is the analysis of pressure performances caused by the fracture dynamics and polymer rheology, as well as an analysis method that derives formation and fracture parameters based on the pressure and its derivative curves.

© 2023 The Authors. Publishing services by Elsevier B.V. on behalf of KeAi Communications Co. Ltd. This is an open access article under the CC BY-NC-ND license (http://creativecommons.org/licenses/by-nc-nd/4.0/).

1. Introduction

As a mature tertiary oil recovery technique, polymer flooding has been widely applied in the development of onshore and offshore oilfields, which effectively increases oil production and reduces water production (Clarke et al., 2016; Wang et al., 2019a; Firozjaii and Saghafi, 2020; Seright and Wang, 2023). Compared with conventional water or gas injection, the viscoelastic polymer

solution exhibits shear thinning and shear thickening characteristics during the flow in porous media, resulting in a wide range of viscosity changes at different shear rates and strong non-linearity flow behavior (Azad and Trivedi, 2019; Li et al., 2019; Shende et al., 2021). Simultaneously, due to the easy adsorption and retention of polymer molecules and solid particles carried during polymer flooding, the porosity and effective permeability of porous media decrease, leading to more complex flow characteristics during polymer flooding (Park et al., 2015; Zhang et al., 2019; Abdelgawad, 2022). Well testing, as an economical and effective method, is widely used in the industry to evaluate the well

E-mail address: petroyang@163.com (Y. Wang).

^{*} Corresponding author.

performance and reservoir characteristics based on the bottomhole pressure data (Gringarten, 2008; Wang et al., 2019b).

In the 1980s, Vongvuthipornchai and Raghavan (1987) applied the numerical simulation module developed by Murtha and Ertekin (1983) to establish an infinite-conductivity polymer-fractured well testing model, assuming the formation fluid is a power-law fluid. They used finite difference method in a two-dimensional Cartesian grid for discrete solutions and analyzed typical well testing curves for power-law fluid fractured wells. Ertekin et al. (1987) established a composite well testing model for finite-conductivity fractured well considering the non-Newtonian/Newtonian behavior of polymer solution. Xu et al. (2003) established a non-Newtonian composite testing model, with the inner region representing the fractured area and the outer region representing a homogeneous formation. The fluid was a single-phase power-law fluid, and they obtained an analytical solution in Laplace space, van den Hoek (2012) presented a practical interpretation method in polymer fall-off tests, from which the in-situ polymer rheology, flow behavior index, and fracture dimensions could be easily estimated. Jia et al. (2015, 2016) developed a numerical testing model for polymer flooding well based on PEBI grid, and studied the impact of shear thinning on typical curves. Ma and McClure (2017) coupled the hydraulic fracturing and reservoir simulation considering the polymer rheology effect, which illustrates that the shear-thickening polymer rheology may significantly reduce well injectivity. Kamal et al. (2019) proposed an analytical solution for pressure transient response in two-phase flow by combining the non-Newtonian fluids and the multi-composite reservoir models. Ukwuigwe and Igbokovi (2021) presented a general solution for two-region composite reservoir, which is applicable to both the Newtonian and non-Newtonian fluids.

However, due to uneven sand placement during fracturing, and geological and engineering factors such as reservoir heterogeneity, formation damage, proppant breakage, and so on, the flux density and fracture conductivity along the hydraulic fracture are non-uniform. Millheim (1968) found that the fracture half-length obtained from well testing interpretation is much smaller than the designed fracture half-length, and speculated that this is due to the low density of proppant distribution. Patankar et al. (2002) studied the influence of proppant migration and settling in hydraulic fractures on the uneven distribution of fracture conductivity. Based on the phenomenon of non-uniform fracture conductivity during the fracture, Huang et al. (2017) and Qin et al. (2019) developed the analysis methods for the pressure transient performances in fractured wells, and the results are consistent with the understanding of formation and fracture characteristics.

Currently, the pressure transient analysis for polymer flooding fracturing well is mainly based on the single-phase power-law fluids, which simplifies the physical and rheological properties of polymer solution in the porous media, and neglects the characteristics of oil-water two-phase flow and the impact of nonuniform fracture conductivity effects. To fill this gap, an oil—water two-phase pressure transient analysis model is established by considering the characteristics of non-uniform fracture conductivity and comprehensive effects of shear thickening, shear thinning, convection, diffusion, adsorption retention, inaccessible pore volume, and reduced effective permeability caused by polymer solution in porous media. The local grid refinement is employed in the near-wellbore region to accurately calculate the pressure distribution and shear rate of polymer solution. Type curves are obtained to investigate the main influence factors on bottom-hole pressure responses in polymer flooding process. Finally, the reliability and practicality of the method are validated through a field case.

2. Methodology

It is well acknowledged that the fracture conductivity is not uniform along the hydraulic fractures, even though it is generally ignored in the pressure transient behavior analysis. This may result in the fracture half-length determined from pressure transient analysis and reservoir simulation history matching are less than the designed fractures. This section involves the main assumptions and mathematical model of non-uniform conductivity fractured wells in viscoelasticity polymer flooding. The oil—water two-phase flow and the characterization of polymer, including the effects of shear thickening, shear thinning, convection, diffusion, adsorption retention, inaccessible pore volume, reduced effective permeability, are considered.

2.1. Assumptions

To facilitate the model development, several assumptions are made as follows:

- (1) The reservoir is homogeneous, isotropic, and of uniform thickness, with uniform distribution of initial formation pressure, water saturation, and polymer concentration.
- (2) The fractures penetrate the formation vertically, distributed symmetrically on both sides of the wellbore, with nonuniform fracture conductivity at various locations.
- (3) Oil—water two-phase flow is considered, with the polymer dissolved in the water phase.
- (4) The effects of shear thickening, shear thinning, convection, diffusion, and adsorption retention of polymers are considered. Meanwhile, we also take into accounts of permeability reduction of water phase caused by the polymer adsorption, and the inaccessible pore volume due to the large molecular size and flexible structure of polymer.
- (5) Oil and water flow in the matrix and fracture obeys Darcy's
- (6) The reservoir fluids and rocks are slightly compressible.
- (7) Chemical reactions during polymer flooding process are neglected, and temperature changes are ignored.

Even though the actual fracture conductivity is space-varying, it is extremely difficult, or we say impossible, to calculate the fracture parameters reliably based on the measured pressure data due to the multiplicity of solutions. To simplify processing for engineering application, the fracture is divided into two parts: high-conductivity fracture near the wellbore and low-conductivity fracture in the far-wellbore section.

2.2. Mathematical model

The continuity equations for oil, water and polymer in the near-wellbore fracture system are

$$\frac{\partial}{\partial t} \left(\phi_{f1} b_{\alpha} S_{f1\alpha} \right) + \nabla \cdot \left(b_{\alpha} v_{f1\alpha} \right) - Q_{\alpha} = 0, \ \alpha = \{ o, w \}, \tag{1}$$

$$\begin{split} &\frac{\partial}{\partial t} \left[\phi_{f1} b_w S_{f1w} C_{f1p} \right] + \nabla \cdot \left(b_w \nu_{f1w} C_{f1p} \right) + \nabla \cdot \left(\nu_{f1d} \right) - Q_w C_{f1p} \\ &= 0. \end{split} \tag{2}$$

The continuity equations for oil, water and polymer in the farwellbore fracture system are

$$\frac{\partial}{\partial t} \left(\phi_{f2} b_{\alpha} S_{f2\alpha} \right) + \nabla \cdot \left(b_{\alpha} v_{f2\alpha} \right) = 0, \tag{3}$$

$$\frac{\partial}{\partial t} \left[\phi_{f2} b_{w} S_{f2w} C_{f2p} \right] + \nabla \cdot \left(b_{w} v_{f2w} C_{f2p} \right) + \nabla \cdot \left(v_{f2d} \right) = 0. \tag{4}$$

The continuity equations for oil, water and polymer in the matrix system are

$$\frac{\partial}{\partial t}(\phi_{m}b_{\alpha}S_{m\alpha}) + \nabla \cdot (b_{\alpha}\nu_{m\alpha}) - Q_{\alpha} = 0, \tag{5}$$

$$\begin{split} &\frac{\partial}{\partial t} \left[\phi_{m} f_{p} b_{w} \left(S_{mw} C_{mp} + \hat{C}_{mp} \right) \right] + \nabla \cdot \left(b_{w} \nu_{mw} C_{mp} \right) + \nabla \cdot \left(\nu_{md} \right) \\ &- Q_{w} C_{mp} \\ &= 0, \end{split}$$

where $\alpha = \{0, w\}$, subscripts o and w represent oil and water, respectively; ϕ_{f1} , ϕ_{f2} , ϕ_m denote the porosities in the near-wellbore fracture, far-wellbore fracture, and matrix, respectively; b_{α} is the reciprocal of volume factor; $S_{f1\alpha}$, $S_{f2\alpha}$, S_m are the saturations in the near-wellbore fracture, far-wellbore fracture, and matrix, respectively; Q_{α} is the flow rate in the wellbore; C_{f1p} , C_{f2p} , C_{mp} are the

polymer concentrations in the near-wellbore fracture, far-wellbore

fracture, and matrix, respectively; \hat{C}_{mp} is the adsorption concentration of the polymer in the matrix; $v_{f1\alpha}$, $v_{f2\alpha}$, $v_{m\alpha}$ are the flow rates in the near-wellbore fracture, far-wellbore fracture, and matrix, respectively; v_{f1d} , v_{f2d} , v_{md} are the polymer diffusion rates in the near-wellbore fracture, far-wellbore fracture, and matrix, respectively.

It is difficult for polymer to enter the matrix pores due to its large molecular size and flexible structure in the polymer flooding process. The parameter f_p , which characterizes the ratio of accessible pore volume of polymer to pore volume of reservoir, is introduced and added in Eq. (6).

According to Darcy's law, the oil and water flow rates in the near-wellbore fracture can be expressed as:

$$v_{\rm flo} = -\frac{K_{\rm fl}k_{\rm ro}}{\mu_{\rm o}} \Big(\nabla p_{\rm flo} \Big), \tag{7}$$

$$v_{\rm flw} = -\frac{K_{\rm fl} k_{\rm rw}}{\mu_{\rm weff} R_{\rm k}} \Big(\nabla p_{\rm flw} \Big). \tag{8}$$

Similarly, the oil and water flow rates in the far-wellbore fracture are

$$v_{f2o} = -\frac{K_{f2}k_{ro}}{\mu_o} \left(\nabla p_{f2o}\right),\tag{9}$$

$$v_{\rm f2w} = -\frac{K_{\rm f2}k_{\rm rw}}{\mu_{\rm weff}R_{\rm k}} \Big(\nabla p_{\rm f2w}\Big). \tag{10}$$

The oil and water flow rates in the matrix are

$$\nu_{\text{mo}} = -\frac{K_{\text{m}}k_{\text{ro}}}{\mu_{\text{o}}}(\nabla p_{\text{mo}}),\tag{11}$$

$$v_{\rm mw} = -\frac{K_{\rm m}k_{\rm rw}}{\mu_{\rm weff}R_{\rm k}}(\nabla p_{\rm mw}). \tag{12}$$

The polymer diffusion rates in the near-wellbore fracture, far-wellbore fracture, and matrix are

$$v_{\rm f1d} = -D_{\rm p}\phi_{\rm f1}S_{\rm f1w}(\nabla C_{\rm f1p}),\tag{13}$$

$$v_{f2d} = -D_p \phi_{f2} S_{f2w} \left(\nabla C_{f2p} \right), \tag{14}$$

$$v_{\rm md} = -D_{\rm p}\phi_{\rm m}f_{\rm p}S_{\rm mw}(\nabla C_{\rm mp}). \tag{15}$$

where $K_{\rm fl}$, $K_{\rm f2}$ denote the absolute fracture permeabilities in the near- and far-wellbores, respectively; $k_{\rm ro}$, $k_{\rm rw}$ represent the relative permeabilities for oil and water, respectively; $p_{\rm fl\,\alpha}$, $p_{\rm fl\,\alpha}$ are the pressures in the near- and far-wellbores, respectively; $\mu_{\rm 0}$ is the oil viscosity; $\mu_{\rm weff}$ is the effective water viscosity; $R_{\rm k}$ is the effective water permeability reduction coefficient; $D_{\rm p}$ is the polymer diffusion coefficient.

The oil and water phase flow rate equations in the near-wellbore fracture are

$$Q_{\alpha} = \frac{2\pi \left| K_{f1} \right| \lambda_{\alpha} a_{f1} b_{\alpha}}{\ln(r_{e}/r_{w}) + S} \left(p_{wf} - p_{f1\alpha} \right) + C b_{\alpha} \frac{\mathrm{d}p_{wf}}{\mathrm{d}t}, \tag{16}$$

with

(6)

$$\lambda_{\mathbf{o}} = \frac{k_{\mathbf{ro}}}{\mu_{\mathbf{o}}},$$

$$\lambda_{\mathsf{W}} = \frac{k_{\mathsf{rW}}}{\mu_{\mathsf{Weff}} R_{\mathsf{k}}}$$

where a_{f1} is the near-wellbore fracture aperture; r_{w} is the well radius; S is the skin factor; p_{wf} is the bottom-hole pressure; C is the wellbore storage coefficient.

The adsorption concentration of the polymer in the matrix system is estimated based on Langmuir adsorption equation as:

$$\hat{C}_{p} = \frac{\hat{C}_{pmax}b_{p}C_{p}}{1 + b_{p}C_{p}}.$$
(17)

The effective water permeability reduction coefficient caused by polymer adsorption is characterized by Hou et al. (2003) as:

$$R_{\rm k} = 1 + \frac{(R_{\rm kmax} - 1)b_{\rm p}C_{\rm p}}{1 + b_{\rm p}C_{\rm p}}, \tag{18}$$

where $\stackrel{\wedge}{C}_{pmax}$ is the maximum adsorption concentration of polymer in the matrix; b_p is a constant; C_p is the injected polymer concentration; R_{kmax} is the maximum permeability decline coefficient.

The initial conditions for reservoir pressure, water saturation, polymer concentration are

$$p_{\alpha}(x,y,z,0) = p_{i}, \tag{19}$$

$$S_{W}(x, y, z, 0) = S_{Wi},$$
 (20)

$$C_{\rm p}(x,y,z,0) = C_{\rm pi}(x,y,z).$$
 (21)

Assuming the outer boundaries are closed, we have

$$\left. \frac{\partial p_{\alpha}}{\partial x} \right|_{x=0,x_{\text{max}}} = \left. \frac{\partial p_{\alpha}}{\partial y} \right|_{y=0,y_{\text{max}}} = \left. \frac{\partial p_{\alpha}}{\partial z} \right|_{y=0,z_{\text{max}}} = 0.$$
 (22)

Combining the saturation equation and capillary pressure equation gives

$$S_W + S_0 = 1,$$
 (23)

$$p_{\text{cow}} = p_{\text{w}} - p_{\text{o}}, \tag{24}$$

where p_i is the initial reservoir pressure; S_{wi} is the initial water saturation; C_{pi} is the initial polymer concentration; p_{cow} is the capillary pressure; x, y, z are the coordinate axis directions; x_{max} , y_{max} , z_{max} are the maximum value in the x, y, z directions, respectively.

The unified viscosity model for polymer solutions proposed by Delshad et al. (2008) is applied, which can characterize the shear viscosity and tensile viscosity of polymers as:

$$\mu_{\text{weff}} = \mu_{\text{sh}} + \mu_{\text{el}},\tag{25}$$

with

$$\mu_{\rm sh} = \mu_{\rm w} + \left(\mu_{\rm p}^0 - \mu_{\rm w}\right) \left[1 + (\lambda_1 \gamma)^2\right]^{\frac{n_1 - 1}{2}},$$
 (26)

$$\mu_{el} = \mu_{max} \left\{ 1 - \exp\left[-\left(\lambda_2 \tau_{\Gamma} \gamma\right)^{n_2 - 1} \right] \right\}, \tag{27}$$

where $\mu_{\rm sh}$ denotes the shear viscosity of polymer; $\mu_{\rm el}$ is the elongational viscosity of polymer; $\mu_{\rm w}$ is the water viscosity; γ is the shear rate of polymer; $\mu_{\rm p}^0$ is the zero shear viscosity of polymer; $\tau_{\rm r}$ is the relaxation time of polymer; $\mu_{\rm max}$, n_1 , n_2 , λ_1 , λ_2 are the empirical constants. Fig. 1 shows the comparison of the apparent polymer viscosity with and without shear thickening (Zhang et al., 2021). It can be found that the polymer viscosity remains basically constant at low shear rate, and then decreases continuously as the shear rate increases. When the shear rate is greater than a critical value, the effective polymer viscosity begins to show an upward trend with the increase in shear rate, which is called shear thickening.

3. Results and discussion

3.1. Numerical implementation

A hybrid grid system, including PEBI mesh and Cartesian grid, is applied to solve the partial differential flow equations. Since the near-well zone has a large pressure gradient and shear thickening of the polymer solution mainly occurs in this area, it is crucial to refine the grid in the near-well zone. The Cartesian grids of large size are distributed far from the wellbore to reduce the

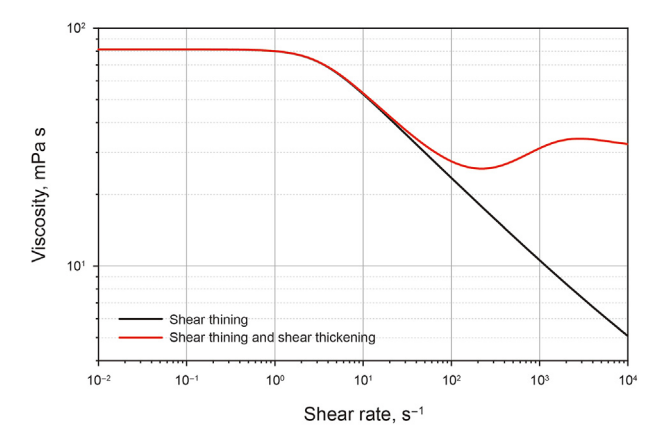


Fig. 1. Comparison of the apparent polymer viscosity with and without shear thickening behavior (Zhang et al., 2021).

computation time (Fig. 2). Fig. 2 shows the hybrid grid for the non-uniform fracture conductivity case, where the black circle represents the wellbore, the blue lines represent the fractures in the near-wellbore section, and the green lines represent the fractures in the far-wellbore section.

The finite volume method is employed to discretize the partial differential equations in mathematical model section. The discretization of Eqs. (1) and (2) for oil, water and polymer in the nearwellbore fracture system can be written as follows:

$$\begin{split} &\frac{\left(\phi_{f1}b_{\alpha}S_{f1\alpha}\right)^{n+1,l}-\left(\phi_{f1}b_{\alpha}S_{f1\alpha}\right)^{n}}{\Delta t^{n+1}}+\operatorname{div}\left(b_{\alpha}v_{f1\alpha}\right)^{n+1,l}-\left(Q_{\alpha}\right)^{n+1,l}\\ &=0, \end{split} \tag{28}$$

$$\begin{split} & \frac{\left(\phi_{f1}b_{w}S_{f1w}C_{f1p}\right)^{n+1,l} - \left(\phi_{f1}b_{w}S_{f1w}C_{f1p}\right)^{n}}{\Delta t^{n+1}} \\ & + \operatorname{div}\left(b_{w}v_{f1w}C_{f1p}\right)^{n+1,l} + \operatorname{div}\left(v_{f1d}\right)^{n+1,l} - \left(Q_{w}C_{f1p}\right)^{n+1,l} \\ & = 0, \end{split}$$
 (29)

where *n* is the time step; and *l* is the iteration step of each time step. Similarly, we can also derive the discretization equations for oil, water and polymer in the far-wellbore fracture system and matrix. Eq. (30) shows the discretization of continuity equations for polymer in the matrix system which considers the effects of polymer diffusion, adsorption retention, and inaccessible pore volume.

$$\frac{\left\{\phi_{m}f_{p}b_{w}\left(S_{mw}C_{mp}+\hat{C}_{mp}\right)\right\}^{n+1,l}-\left\{\phi_{m}f_{p}b_{w}\left(S_{mw}C_{mp}+\hat{C}_{mp}\right)\right\}^{n}}{\Delta t^{n+1}} + \operatorname{div}\left(b_{w}v_{mw}C_{mp}\right)^{n+1,l}+\operatorname{div}\left(v_{md}\right)^{n+1,l}-\left(Q_{w}C_{mp}\right)^{n+1,l}} = 0.$$
(30)

The oil and water phase flow rate equations in the near-wellbore fracture can be written as

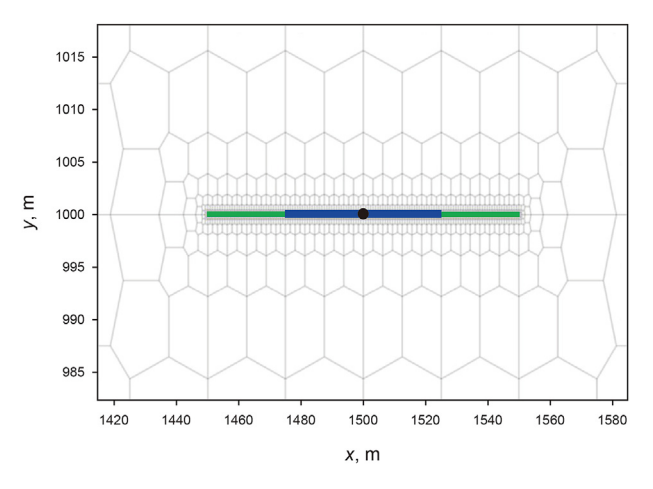


Fig. 2. Diagram of a fracture with non-uniform conductivity in a fractured vertical well system.

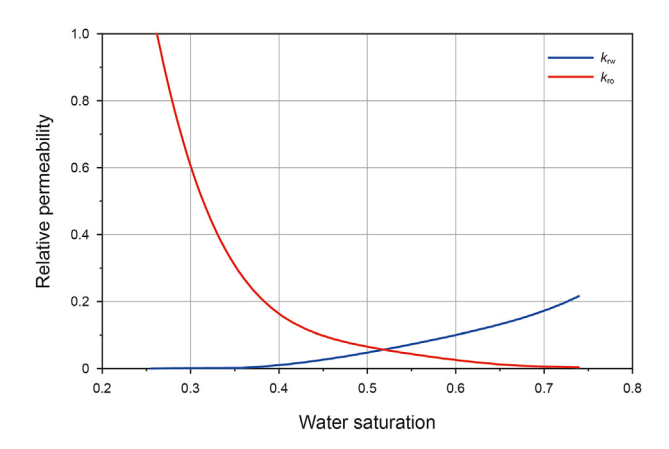


Fig. 3. Relative permeability curve.

$$Q_{\alpha}^{n+1,l} = \left\{ \frac{2\pi \left| K_{f1} \right| \lambda_{\alpha} a_{f1} b_{\alpha}}{\ln(r_{e}/r_{w}) + S} \right\}^{n+1,l} \left(p_{wf} - p_{f1\alpha} \right)^{n+1,l} + \left\{ C b_{\alpha} \right\}^{n+1,l} \frac{p_{wf}^{n+1,l} - p_{wf}^{n}}{\Delta t^{n+1}}.$$
(31)

Other equations are easily formulated in the similar way. Finally, the equations can be solved by the automatic differentiation and Newton iteration method, which is programmed based on MATLAB codes.

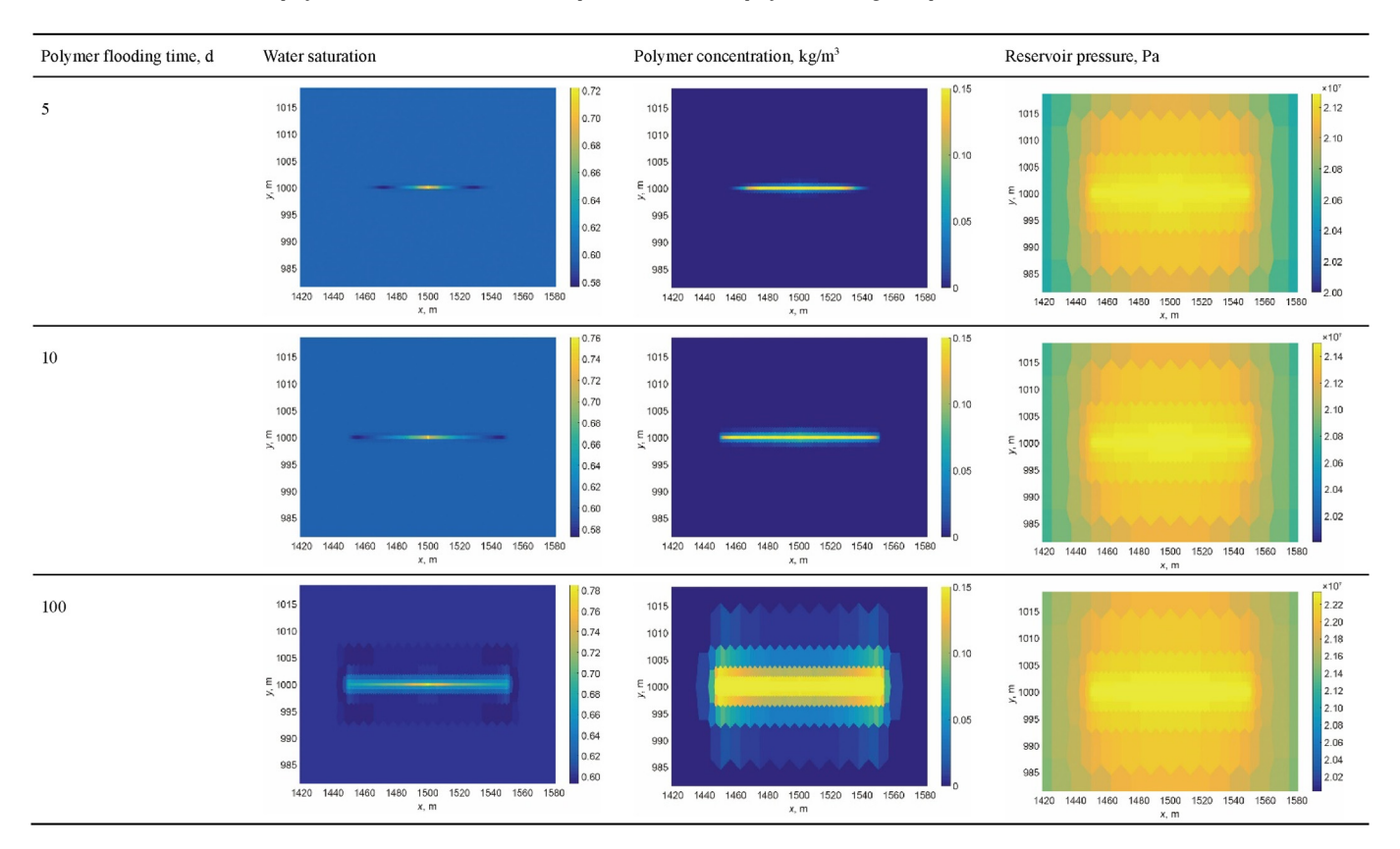
3.2. Flow behavior of polymer flooding

To illustrate the influence of non-uniform fracture conductivity on the pressure and polymer concentration distribution during polymer flooding, a 3000 m \times 3000 m \times 10 m homogeneous reservoir is designed, with the fractured polymer injection well located at the center of the reservoir. The fracture half-lengths in the near-well and far-well sections are both 25 m. The fracture conductivity coefficients are 60 µm² m for the near-wellbore section and $12 \, \mu m^2$ m for the far-wellbore section. The injection rate of the polymer solution is 100 m³/d, the initial polymer concentration of the reservoir is 0 kg/m³, and the injected polymer concentration is 0.15 kg/m³. The relative permeability curves for oil and water are shown in Fig. 3, and the polymer parameters (Zhang et al., 2021) are applied. The distribution of water saturation, polymer concentration, and formation pressure can be calculated by the above gridding and numerical solution methods. Table 1 shows the field distribution of polymer injection for 5, 10, and 100 d. It is found that the injected polymer fills the fracture first, and then flow perpendicular to the fracture towards the formation. The effective sweep distance of polymer flooding is limited according to the polymer concentration variation field.

3.3. Type curve and sensitivity analysis

Type curve of viscoelastic polymer flooding fracturing wells with non-uniform fracture conductivity are presented in the log—log plot (Fig. 4), which can be divided into five flow regimes: wellbore storage, transitional flow, bilinear flow, linear flow, and

Table 1Distribution of water saturation, polymer concentration and reservoir pressure in different polymer flooding time periods.



radial flow. Our model is degenerated into uniform conductivity fracture model when the fracture conductivity in the far-wellbore section is set equal to the near-wellbore section as 60 μm^2 m, whose type curve is also plotted in Fig. 4. This situation is comprehensively discussed and validated in our previous paper (Wang et al., 2023). Compared with the polymer flooding well with uniform fracture conductivity, the non-uniform fracture conductivity case exhibits the larger pressure difference, and the shorter bilinear flow period due to the decrease in fracture flow ability in the far-wellbore section. The linear flow regime appears earlier, and the radial flow dominates faster. The effect of polymer rheology is largely reflected in the calculation of viscosity. Compared with waterflooding, the viscosity of polymer solution is much bigger, which results in larger pressure loss. Meanwhile, the effect of shear thickening is also discussed in our paper. The pressure and its derivatives calculated by considering both shear thinning and shear thickening are significantly greater than those calculated without considering shear thickening. This is because the high shear rate near the wellbore demonstrates the shear thickening characteristics of the polymer solution, causing an increase in the viscosity of the polymer solution near the wellbore.

To analyze the impacts of non-uniform fracture conductivity distribution and the polymer characteristics on the type curves during polymer flooding, the effects of the ratio of fracture lengths, fracture conductivities between the near-wellbore and far-wellbore sections, polymer concentration, and water saturation are investigated. The total fracture length, including the near-wellbore and far-wellbore sections, is 100 m. The fracture conductivity in the near-wellbore section is $60 \ \mu m^2 \ m$.

Fig. 5 shows the impact of the ratio of fracture lengths between the near-wellbore and far-wellbore sections $(f_1|f_2)$ on the type curves of polymer flooding wells. It is found that the relative fracture length in the near- and far-wellbore sections has a big impact on the bottom-hole pressure behavior. Results show that the pressure difference is larger, the transitional flow and bilinear flow regimes become shorter, and the linear flow regime appears earlier as the increase in the fracture length in the far-wellbore section. Meanwhile, the analysis reveals that the $f_1|f_2$ has no impact on the pressure-derivative value in radial flow, which is influenced by formation permeability, but affects the time to achieve radial flow.

To magnify the impact of fracture conductivity on the bottomhole pressure responses, the ratios of fracture conductivities between the near-wellbore and far-wellbore sections ($C_{\rm f1}/C_{\rm f2}$) are set as 1, 10, and 100, and the fracture lengths for near- and far-wellbore sections are keep the same as 50 m. The pressure performance for different cases is shown in Fig. 6, which behaves similarly with

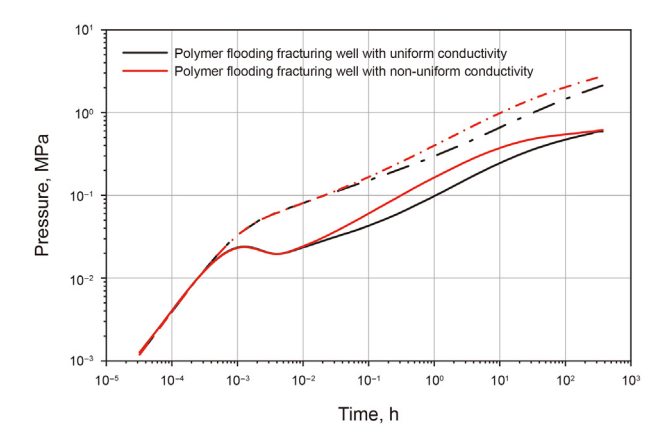


Fig. 4. Comparison of type curves between the polymer flooding well with non-uniform and uniform conductivity fractures.

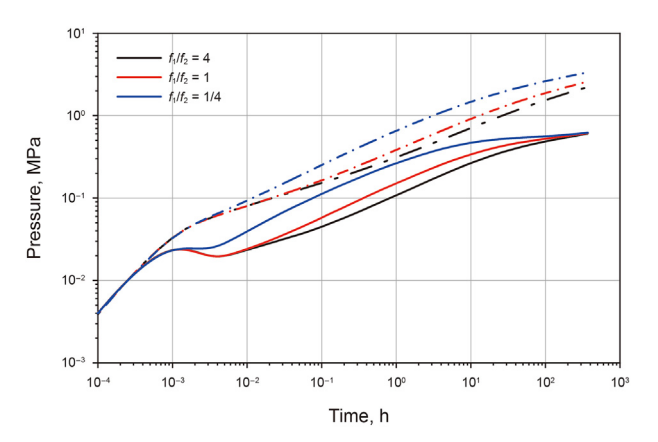


Fig. 5. Influence of f_1/f_2 on bottom-hole pressure performance.

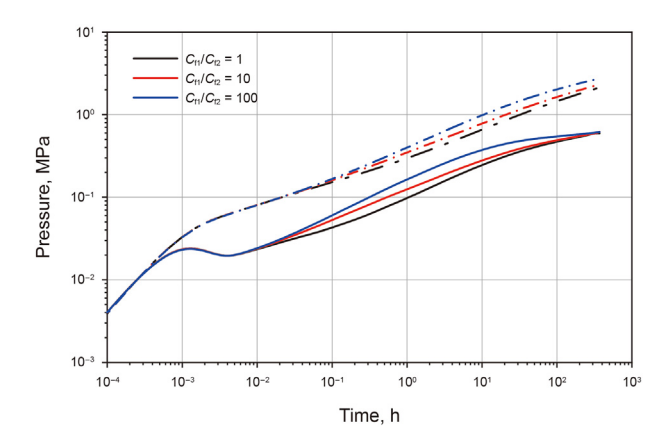


Fig. 6. Influence of C_{f1}/C_{f2} on bottom-hole pressure performance.

fracture length. As the decrease in fracture conductivity in the farwellbore section, the pressure difference becomes larger, the transitional flow and bilinear flow regimes become shorter, and the linear flow regime appears earlier. The sensitivity analysis for the ratio of fracture lengths, fracture conductivities between the nearwellbore and far-wellbore sections in Figs. 6 and 7 demonstrates the significant influence of the non-uniform fracture conductivity parameters on bottom-hole pressure responses, which further

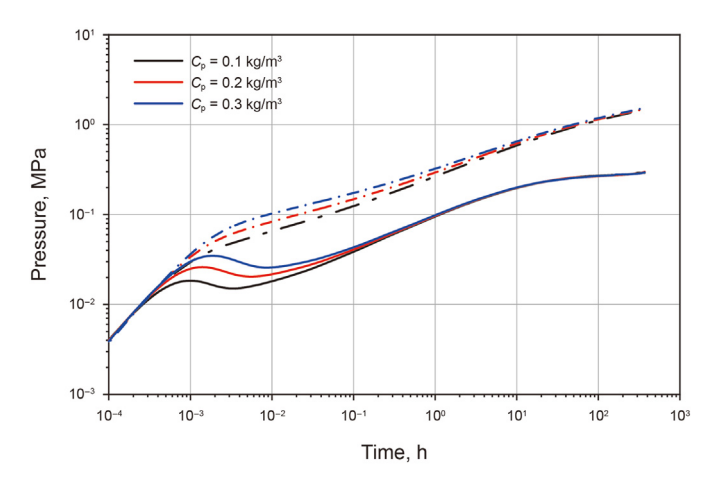


Fig. 7. Influence of injected polymer concentration on bottom-hole pressure performance.

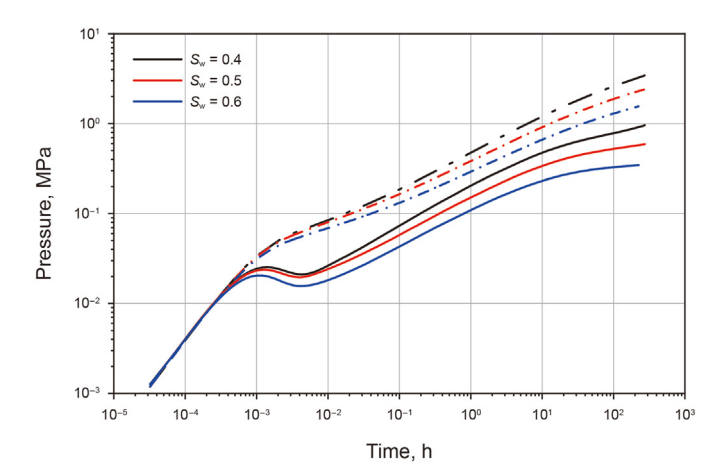


Fig. 8. Influence of water saturation on bottom-hole pressure performance.

confirms the necessity of considering this effect.

Fig. 7 shows the impact of injected polymer concentration on the bottom-hole pressure transient behavior. It can be observed that the pressure and its derivative curves in the transitional flow section shift upwards, and the range of bilinear flow shortens with the increase in the injected polymer solution concentration. The water phase viscosity increases in the near-well zone as the increase in polymer solution concentration, which leads to larger pressure loss.

Water saturation is one of the key influence parameters for

oil—water two-phase flow pressure transient analysis, which differs with classical well testing analysis where single-phase flow is generally assumed. It can be concluded from Fig. 8 that the pressure and its derivative curves shift downwards after wellbore-storage regime with the increase in water saturation. As we all know, the water-phase relative permeability increases, and the oil-phase relative permeability decreases as the increase in water saturation. Due to the fact that the water viscosity is much less than oil, the increase in water mobility is much greater than the decrease in oil mobility, resulting in the increase in total mobility. Therefore, the pressure loss is reduced as the increase in water saturation.

4. A field case

A polymer flooding fracturing well is presented in this part to illustrate the applicability of the methodology. The formation and fluid parameters are provided in Table 2. No faults or bottom water are identified near the well. The block was converted from water flooding to polymer flooding in September 2019, and the injection well was shut in 70.29 h for pressure fall-off test on April 19, 2021. Considering that neighboring production wells had already started producing polymer, the initial polymer concentration in the reservoir was assumed to be close to the polymer concentration in the neighboring production wells. The measured bottom-hole pressure data is shown in Fig. 9. Different theoretical well test curves are calculated to match the measured pressure data until the matching accuracy meets the requirements by adjust the parameters, including wellbore storage coefficient, matrix permeability, fracture half-lengths and conductivities in the near- and far-

Table 2Basic parameters of the fall-off test for polymer flooding fracturing well.

Parameter	Value
Porosity, %	15.8
Rock compressibility, MPa ⁻¹	1.27×10^{-3}
Formation thickness, m	19.5
Well radius, m	0.07
Initial water saturation, %	71
Water viscosity, mPa s	0.99
Oil viscosity, mPa s	5.84
Water compressibility, MPa ⁻¹	1.5×10^{-4}
Oil compressibility, MPa ⁻¹	2.1×10^{-3}
Water volume coefficient, m ³ /m ³	1.001
Oil volume coefficient, m ³ /m ³	1.174
Injection flow rate, m ³ /d	42
Injected polymer concentration, kg/m ³	0.6
Polymer concentration produced by adjacent production well, kg/m ³	0.37

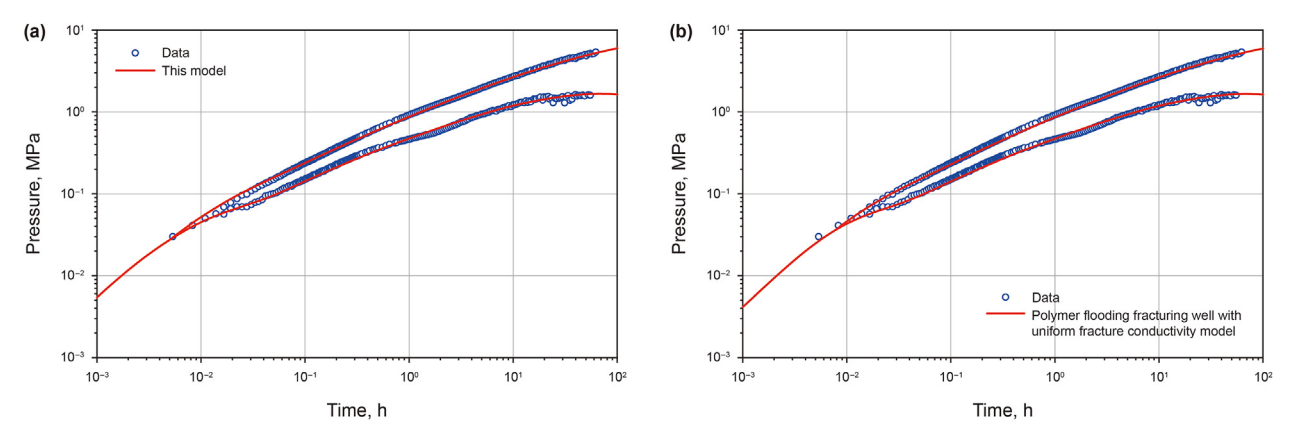


Fig. 9. log-log matching plot. (a) This model; (b) Polymer flooding fracturing well with uniform fracture conductivity model.

Table 3Comparison results of the polymer flooding well with uniform and un-uniform fracture conductivity.

Results	This model	Polymer flooding well with uniform fracture conductivity model
Wellbore storage coefficient, m ³ /MPa	0.76	0.76
Fracture half-length in the near-wellbore section, m	9.4	
Fracture half-length in the far-wellbore section, m	37.6	
Total fracture half-length, m	47.0	29.5
Fracture conductivity coefficient in the near-wellbore section, μm^2 m	360	590
Fracture conductivity coefficient in the far-wellbore section, μm^2 m	170	590
Matrix permeability, $10^{-3} \mu m^2$	18	17

wellbore sections, and so on. To decrease the multiplicity of the interpretation, we first need to confirm the determined parameters (e.g. the parameters presented in Table 2), and uncertain parameters (e.g. fracture half-length, fracture conductivity, permeability, and so on). Then, the parameter ranges are defined to constrain the uncertain parameters. Finally, the interpretation results should be checked according to the well-known results (e.g. the average permeability, maximum fracture length, and so on). The log-log matching plot is shown in Fig. 9(a) and the interpretation results are provided in Table 3. For comparison purpose, the polymer flooding fracturing well with uniform fracture conductivity model (Wang et al., 2023) is also applied to interpret the pressure data. The pressure matching plot is shown in Fig. 9(b) and the results are provided in Table 3. It can be observed that the interpreted fracture half-length is 29.5 m by polymer flooding fracturing well with uniform fracture conductivity model, which is much smaller than the designed fracturing half-length (50 m), even though it also has a good matching effect in Fig. 9(b). However, the model proposed in this paper yields a more reasonable fracture half-length of 47 m, including 9.4 m near-wellbore fracture and 37.6 m far-wellbore fracture. This value is more consistent with the designed fracturing half-length. In the previous model, the pressure transient analysis method for polymer flooding fracturing well is established by considering the complex characteristics of polymer solution and oil-water two-phase flow. We have shown that the matrix permeability obtained by the model is closer to the true value than conventional fractured well which assumes single water-phase flow. In this paper, we work step further by considering the nonuniform feature of hydraulic fractures based on the previous model, which achieves the segmented characterization of high- and low-conductivity fracture in the near- and far-wellbore section. respectively.

5. Conclusions

- (1) The pressure transient method of non-uniform conductivity fracture well in viscoelasticity polymer flooding is established based on the theory of oil—water two-phase flow, which considers the comprehensive effects of shear thickening, shear thinning, convection, diffusion, adsorption retention, inaccessible pore volume, and reduced effective permeability in polymer flooding. A hybrid grid system, including PEBI mesh and Cartesian grid, is applied to solve the partial differential flow equations and derive the type curves.
- (2) Compared with the polymer flooding well with uniform fracture conductivity, the model presented in this paper exhibits an upward pressure and pressure derivative curve after the transitional flow regime, a shortened duration of the bilinear flow regime, and an earlier entry into the linear flow and radial flow regimes. This characteristic becomes more pronounced with the increase in the fracture length or the decrease in fracture conductivity in the far-wellbore section.

- The differences in the linear flow regime cause the fracture parameters obtained by the polymer flooding well with uniform fracture conductivity model to deviate from reality.
- (3) Results from the pressure fall-off test in the polymer flooding fracturing well show that the fracture half-length obtained by the model proposed in this paper is more consistent with the designed fracturing length, further confirming the reliability and practicality of the polymer flooding fracturing well testing analysis method. It achieves a quantitative segmented characterization of the near-wellbore section with high fracture conductivity and the far-wellbore section with low fracture conductivity.

CRediT authorship contribution statement

Yang Wang: Formal analysis. **Jia Zhang:** Investigation. **Shi-Long Yang:** Validation. **Ze-Xuan Xu:** Writing — original draft. **Shi-Qing Cheng:** Supervision, Writing — review & editing.

Declaration of competing interest

The authors declare that they have no known competing financial interests or personal relationships that could have appeared to influence the work reported in this paper.

Acknowledgements

This work is supported by the National Natural Science Foundation of China (No. 52104049), the Young Elite Scientist Sponsorship Program by Beijing Association for Science and Technology (No. BYESS2023262), and Science Foundation of China University of Petroleum, Beijing (No. 2462022BJRC004).

References

- Abdelgawad, K.Z., 2022. Polymer induced permeability reduction: the influence of polymer retention and porous medium properties. J. Petrol. Sci. Eng. 217, 110821. https://doi.org/10.1016/j.petrol.2022.110821.
- Azad, M.S., Trivedi, J.J., 2019. Quantification of the viscoelastic effects during polymer flooding: a critical review. SPE J. 24 (6), 2731–2757. https://doi.org/10.2118/195687-PA
- Clarke, A., Howe, A.M., Mitchell, J., et al., 2016. How viscoelastic-polymer flooding enhances displacement efficiency. SPE J. 21 (3), 675–687. https://doi.org/ 10.2118/174654-PA.
- Delshad, M., Magbagbeola, O.A., Huh, C., et al., 2008. Mechanistic interpretation and utilization of viscoelastic behavior of polymer solutions for improved polymerflood efficiency. In: SPE Symposium on Improved Oil Recovery. https://doi.org/ 10.2118/113620-MS.
- Ertekin, T., Cicek, O., Adequmi, M.A., et al., 1987. Pressure transient behavior of non-Newtonian/Newtonian fluid composite systems in porous media with a finite conductivity vertical fracture. In: SPE Eastern Reg. Meet. https://doi.org/10.2118/17053-MS.
- Firozjaii, A.M., Saghafi, H.R., 2020. Review on chemical enhanced oil recovery using polymer flooding: fundamentals, experimental and numerical simulation. Petroleum 6 (2), 115–122. https://doi.org/10.1016/j.petlm.2019.09.003.
- Gringarten, A.C., 2008. From straight lines to deconvolution: the evolution of the state of the art in well test analysis. SPE Reservoir Eval. Eng. 11 (1), 41–62. https://doi.org/10.2118/102079-PA.

Hou, J., Li, Z., Wang, Y., et al., 2003. Numerical simulation of polymer flooding with dispersion and adsorption. Chin. J. Comput. Phys. 20 (3), 239–244. https://doi: 10.19596/j.cnki.1001-246x.2003.03.010 (in Chinese).

- Huang, Y., Cheng, S., Yu, H., et al., 2017. A semianalytical approach to estimate fracture closure and formation damage of vertically fractured wells in tight gas reservoir. J. Petrol. Sci. Eng. 150, 85–90. https://doi.org/10.1016/ i.petrol.2016.10.049.
- Jia, Z., Li, D., Yang, J., et al., 2015. Numerical well test analysis for polymer flooding considering the non-Newtonian behavior. J. Chem. 2015, 1–10. https://doi.org/ 10.1155/2015/107625.
- Jia, Z., Yan, S., Dong, X., et al., 2016. Numerical study on the impact of shear thinning behavior in well test analysis for polymer flooding. J. SW. Petrol. Univ. (Sci. Technol. Ed.) 38 (5), 107–114. https://doi:10.11885/j.issn.1674-5086.2014.11.28. 02 (in Chinese).
- Kamal, M.M., Tian, C., Suleen, F., 2019. Pressure transient analysis of polymer flooding with coexistence of non-Newtonian and Newtonian fluids. SPE Reservoir Eval. Eng. 22 (3), 1172–1184. https://doi.org/10.2118/181473-PA.
- Li, X., Yin, H., Zhang, R., et al., 2019. A salt-induced viscosifying smart polymer for fracturing inter-salt shale oil reservoirs. Petrol. Sci. 16, 816–829. https://doi.org/ 10.1007/s12182-019-0329-3.
- Ma, Y., McClure, M.W., 2017. The effect of polymer rheology and induced fracturing on injectivity and pressure-transient behavior. SPE Reservoir Eval. Eng. 20 (2), 394–402. https://doi.org/10.2118/184389-PA.
- Millheim, K.K., 1968. Testing and analyzing low-permeability fractured gas wells. J. Petrol. Technol. 20 (2), 193–198. https://doi.org/10.2118/1768-PA.
- Murtha, J.A., Ertekin, T., 1983. Numerical simulation of power-law fluid flow in a vertically fractured reservoir. In: SPE Annual Technical Conference and Exhibition. https://doi.org/10.2118/12011-MS.
- Park, H., Han, J., Sung, W., 2015. Effect of polymer concentration on the polymer adsorption-induced permeability reduction in low permeability reservoirs. Energy 84, 666–671. https://doi.org/10.1016/j.energy.2015.03.028.
- Patankar, N.A., Joseph, D.D., Wang, J., et al., 2002. Power law correlations for sediment transport in pressure driven channel flows. Int. J. Multiphas. Flow 28 (8), 1269–1292. https://doi.org/10.1016/S0301-9322(02)00030-7.
- Qin, J., Cheng, S., Li, P., et al., 2019. Interference well-test model for vertical well with double-segment fracture in a multi-well system. J. Petrol. Sci. Eng. 183, 106412.

- https://doi.org/10.1016/j.petrol.2019.106412.
- Seright, R.S., Wang, D., 2023. Polymer flooding: current status and future directions. Petrol. Sci. 20 (2), 910–921. https://doi.org/10.1016/j.petsci.2023.02.002.
- Shende, T., Niasar, V.J., Babaei, M., 2021. An empirical equation for shear viscosity of shear thickening fluids. J. Mol. Liq. 325, 115220. https://doi.org/10.1016/ j.molliq.2020.115220.
- Ukwuigwe, O.C., Igbokoyi, A.O., 2021. Analytical solution to pressure transient analysis in non-Newtonian/Newtonian fluids in naturally fractured composite reservoirs. J. Pet. Explor. Prod. Technol. 11, 4277—4293. https://doi.org/10.1007/ s13202-021-01292-1
- van den Hoek, P.J., Mahani, H., Sorop, T.G., et al., 2012. Application of injection falloff analysis in polymer flooding. In: SPE Europec/EAGE Annual Conference. https://doi.org/10.2118/154376-MS.
- Vongvuthipornchai, S., Raghavan, R., 1987. Pressure falloff behavior in vertically fractured wells: non-Newtonian power-law fluids. SPE Form. Eval. 2 (4), 573-589. https://doi.org/10.2118/13058-PA.
- Wang, X., Yin, H., Zhao, X., et al., 2019a. Microscopic remaining oil distribution and quantitative analysis of polymer flooding based on CT scanning. Adv. Geo-Energy Res. 3 (4), 448–456. https://doi:10.26804/ager.2019.04.
 Wang, Y., Cheng, S., Zhang, K., et al., 2019b. Investigation on the transient pressure
- Wang, Y., Cheng, S., Zhang, K., et al., 2019b. Investigation on the transient pressure response of water injector coupling the dynamic flow behaviors in the wellbore, waterflood-induced fracture and reservoir: semi-analytical modeling and a field case. Int. J. Heat Mass Tran. 130, 668–679. https://doi.org/10.1016/j.ijheatmasstransfer.2018.09.083.
- Wang, Y., Yu, H., Zhang, J., et al., 2023. Transient pressure analysis of polymer flooding fractured wells with oil—water two-phase flow. Petrol. Explor. Dev. 50 (1), 160—166. https://doi.org/10.11698/PED.20220341.
- Xu, J., Wang, L., Zhu, K., 2003. An analysis of oil well testing for non-Newtonian fluid in a fracture-dominated reservoir. Petrol. Sci. Technol. 21 (9–10), 1381–1393. https://doi.org/10.1081/LFT-120023204.
- Zhang, J., Cheng, S., Zhan, J., et al., 2021. The effect of rheology of viscoelastic polymer on pressure transient response in near-wellbore regions. Geofluids, 5568336. https://doi.org/10.1155/2021/5568336.
- Zhang, J., Cheng, S., Zhu, C., et al., 2019. A numerical model to evaluate formation properties through pressure-transient analysis with alternate polymer flooding. Adv. Geo-Energy Res. 3 (1), 94–103. https://doi:10.26804/ager.2019.01.0.